8-1-2022

Thermodynamic modeling of hydrogen–water systems with gas impurity at various conditions using cubic and PC-SAFT equations of state

Amer Alanazi

Saleh Bawazeer

Muhammad Ali

Alireza Keshavarz
Edith Cowan University, a.keshavarz@ecu.edu.au

Hussein Hoteit

10.1016/j.ecmx.2022.100257
Alanazi, A., Bawazeer, S., Ali, M., Keshavarz, A., & Hoteit, H. (2022). Thermodynamic modeling of hydrogen–water systems with gas impurity at various conditions using cubic and PC-SAFT equations of state. Energy Conversion and Management: X, 15, 100257. https://doi.org/10.1016/j.ecmx.2022.100257

Energy Conversion and Management: X 15 (2022) 100257

Contents lists available at ScienceDirect

Energy Conversion and Management: X

journal homepage: www.sciencedirect.com/journal/energy-conversion-and-management-x

Thermodynamic modeling of hydrogen–water systems with gas impurity at various conditions using cubic and PC-SAFT equations of state

Amer Alanazi [a,*], Saleh Bawazeer [b], Muhammad Ali [a], Alireza Keshavarz [c], Hussein Hoteit [a]

[a] Physical Science & Engineering Division, King Abdullah University of Science and Technology, Thuwal, Saudi Arabia
[b] Mechanical Engineering Department, College of Engineering and Islamic Architecture, Umm Al-Qura University, P.O. 5555, Makkah 24382, Saudi Arabia
[c] School of Engineering, Edith Cowan University, Joondalup 6027, WA, Australia

A R T I C L E I N F O

Keywords:
Hydrogen storage
hydrogen-water
solubility
hydrogen impurity
water vaporization
equation of state (EoS)
fuel cells

A B S T R A C T

Hydrogen (H_2) has emerged as a viable solution for energy storage of renewable sources, supplying off-seasonal demand. Hydrogen contamination due to undesired mixing with other fluids during operations is a significant problem. Water contamination is a regular occurrence; therefore, an accurate prediction of H_2-water thermodynamics is crucial for the design of efficient storage and water removal processes. In thermodynamic modeling, the Peng–Robinson (PR) and Soave Redlich–Kwong (SRK) equations of state (EoSs) are widely applied. However, both EoSs fail to predict the vapor-liquid equilibrium (VLE) accurately for H_2-blend mixtures with or without fine-tuning binary interaction parameters due to the polarity of the components. This work investigates the accuracy of two advanced EoSs: the Schwartzentruber and Renon modified Redlich–Kwong cubic EoS (SR-RK) and perturbed-chain statistical associating fluid theory (SAFT) in predicting VLE and solubility properties of H_2 and water. The SR-RK involves the introduction of polar parameters and a volume translation term. The proposed workflow is based on optimizing the binary interaction coefficients using regression against experimental data that cover a wide range of pressure (0.34 to 101.23 MPa), temperature (273.2 to 588.7 K), and H_2 mole fraction (0.0004 to 0.9670) values. A flash liberation model is developed to calculate the H_2 solubility and water vaporization at different temperature and pressure conditions. The model captures the influence of H_2-gas (CO_2) impurity on VLE. The results agreed well with the experimental data, demonstrating the model's capability of predicting the VLE of hydrogen-water mixtures for a broad range of pressures and temperatures. Optimized coefficients of binary interaction parameters for both EoSs are provided. The sensitivity analysis indicates an increase in H_2 solubility with temperature and pressure and a decrease in water vaporization. Moreover, the work demonstrates the capability of SR-RK in modeling the influence of gas impurity (i.e., H_2–CO_2 mixture) on the H_2 solubility and water vaporization, indicating a significant influence over a wide range of H_2–CO_2 mixtures. Increasing the CO_2 ratio from 20% to 80% exhibited almost the opposite behavior of H_2 solubility compared to the pure hydrogen feed solubility. Finally, the work emphasizes the critical selection of proper EoSs for calculating thermodynamic properties and the solubility of gaseous H_2 and water vaporization for the efficient design of H_2 storage and fuel cells.

Introduction

Hydrogen (H_2) is an attractive clean fuel, enabling the vast expansion of renewable sources toward achieving a net-zero carbon economy [1]. The accelerated growth of the world population is causing an unprecedented increase in energy demand, imposing an additional driver to promote alternatives [2,3]. Outlooks from global energy anticipate about 40% of the worldwide electricity to come from renewable alternatives by 2040 [4]. However, the produced energy from renewable resources, such as wind power and solar, provides only an intermittent supply due to their seasonal nature [5,6]. Hydrogen is anticipated to play a vital role in storing energy from renewables for off-seasonal demand [7–11].

Applications of H_2 in the energy sectors are vast and diverse and include transportation, heating, fuel cells, and petrochemical industrial use [12,13]. Hydrogen is known for its low volumetric energy density attributed to its low density under standard conditions [14–16]. Hydrogen is compressed and cooled for storage and transportation, causing the density to increase significantly [16–18]. Several H_2

* Corresponding author.
E-mail address: Amer.alanazi@kaust.edu.sa (A. Alanazi).

https://doi.org/10.1016/j.ecmx.2022.100257
Received 28 March 2022; Received in revised form 12 June 2022; Accepted 19 June 2022
Available online 21 June 2022

Nomenclature

Symbols

a	Equation term for attraction
b	Equation term for co-volume
c	Volume-shift correction factor or volume translation factor
C_d	Parameter of BM-PR and SR-RK
f	Helmholtz free energy
k_a	Binary interaction parameter for attraction term,a
k_b	Binary interaction parameter for co-volume term,b
k_B	Boltzmann constant
k_{ij}	Binary interaction parameter for components i and j
l_{ij}	Secondary binary interaction parameter for components I and j in the co-volume
m	Parameter of the cubic EoS related to ω
M	Number of molecular chain segments
n, N	Number of data points
P	Pressure
R	Universal gas constant
T	Temperature
V	Volume
V_m	Molar volume
w	Parameter of the general formalism EoS
x	Mole fraction in the liquid phase
$\overline{x}$	Average mole fraction in the liquid phase
X_{ij}	Binary interaction parameter for volume translation,c
y	Mole fraction in the gas phase
$\alpha(T)$	Alpha function in the cubic EoS
δ	Coefficient of the binary interaction
ε	Dispersion energy between segments
ε^{AB}	Association energy between sites or molecules
κ^{AB}	Association volume
ρ	Density
σ	Standard deviation
σ(Å)	Diameter of the chain segment
ω	Acentric factor
Ω_a	Unitless constant of the cubic EoS of a
Ω_b	Unitless constant of the cubic EoS of b

Abbreviation

AAD	Average absolute deviation
BM-PR	Boston–Mathias Peng–Robinson
EoS	Equation of state
MLF	Maximum likelihood function
NG	Number of data groups
NP	Number of data points
NC	Total number of components
PC-SAFT	Perturbed-chain statistical associating fluid theory
PR	Peng–Robinson
RK	Redlich–Kwong
RMSE	Root mean square error
SAFT	Statistical associating fluid theory
SR-RK	Schwartzentruber–Renon Redlich–Kwong
SRK	Soave Redlich–Kwong

Super/subscripts

a	Coefficient parameter for attraction
assoc	Association
b	Coefficient parameter for co-volume
c	Critical
Cal.	Calculated value
disp	Dispersion
e	Estimated
Exp.	Experimental value
g	Gas
hc	Chain formation
hs	Hard-sphere repulsion
i, j	Component labels
l	Liquid
m	Measured
mix	Mixture
polar	Interpolar
r	Reduced
ref	Reference
res	Residual
v	Vapor

compression methods have been proposed for effective storage in fuel cell electric vehicles and electrochemical H_2 compressors [19,20]. The latter is analogous to fuel cells designed based on proton exchange membrane (PEM) technology, where water (H_2O) enables the proton transfer via the membrane (Fig. 1). The advantages of electrochemical H_2 compressors compared to conventional techniques have been extensively reviewed [13,14,19,21]. Nonetheless, a major disadvantage is the necessity to hydrate the membrane with water to enable proton transportation through the membrane. As a result, the generated H_2 is always saturated in water, causing unpremeditated impurities. The International Organization for Standardization (ISO) provided a standard maximum allowable limit of 5 μmol of H_2O per mol of H_2 for the water content in vapor-phase H_2 for PEM fuel cells used in vehicles [14].

However, a large expansion of a H_2-based economy requires massive storage capacity on the terawatt scale [22–24]. Such a scale can be offered by underground storage in geological formations, including salt caverns, depleted hydrocarbon reservoirs, and deep saline aquifers, where gas mixing with reservoir fluids is inevitable [25], as illustrated in Fig. 2. The presence of water co-existing in the transportation and injection process and the uncaptured phase can cause fluctuations in pressure, leading to major cavitation and pipeline damage [26]. Therefore, accurate modeling of water solubility in H_2 and vice-versa is critical for the success of the storage process and the application of transportation and PEM technology.

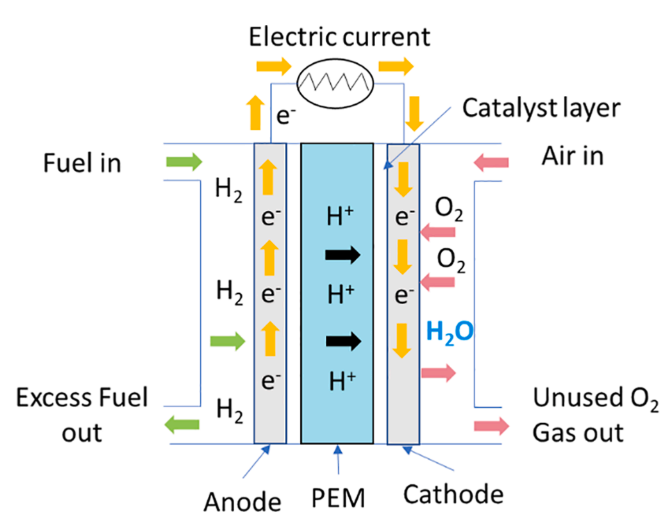

Fig. 1. Schematic of the basic structure of proton exchange membrane (PEM) fuel cell.

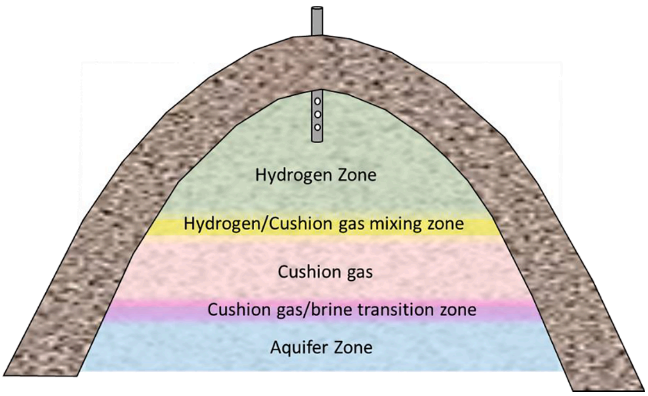

Fig. 2. Illustration of hydrogen storage in an underground geological formation with a cushion gas and an aquifer zone.

The knowledge of pure H_2 thermodynamics is well established [27,28]. However, available experimental data on H_2-blend mixtures does not cover the full range of gas mixtures and H_2 operational conditions for underground storage or fuel cell electric vehicles. Therefore, reliable equations of state (EoSs) are needed to predict these properties.

The cubic EoSs, such as Peng–Robinson (PR) [29] and Soave Redlich–Kwong (SRK) [30], are widely used in compositional reservoir simulators. Several researchers have intensively investigated their reliability [31], where varying accuracy was observed in different conditions. The PR and SRK EoSs are often used with flash calculations to determine equilibrium phases, phase properties, and the compositional flow and transport of each phase [32–36]. However, challenges arise when classical cubic EoSs are used to calculate the phase equilibrium and mixture density at conditions of high pressure and temperature for H_2-blend mixtures. Such predictions become less accurate at high densities caused by the quantization of translational motion and the quantum nature of H_2 [37]. This poor predictability becomes more pronounced when H_2 is mixed with one or more polar components.

In 1949, Redlich and Kwong proposed one of the earliest extensions of the attraction term in the van der Waals EoS [38]. The particle-interaction term was introduced as a temperature-dependent term (i.e., a(T)) to improve the predictions of vapor-liquid equilibria (VLE) for nonideal gases [39]. Later, the alpha function, as a function of reduced temperature, was developed by Wilson [40]. Then, Soave proposed the use of a generalized alpha function [30], leading to the development of the current EoSs, such as SRK. These EoSs use different forms of the temperature-dependent term and an acentric factor (ω) as an additional parameter. A volume correction factor (c) in the alpha function was introduced to improve the accuracy of the density prediction [41,42]. Boston and Mathias extended the range of temperature and pressure by distinguishing the sub- and super-critical regions [43,44]. Mathias (1983) [45] improved the developed relations to cover highly polar substances, such as H_2O, CO_2, and CO, by introducing a polar parameter in the alpha function. Afterward, Schwartzentruber and Renon further improved polar substances by introducing three polar parameters (i.e., p_o, p_1, p_2) [46].

Other types of advanced EoSs have been developed based on statistical mechanics, referred to as statistical associating fluid theory (SAFT). Perturbed-chain SAFT (PC-SAFT) is a widely applied SAFT EoS that uses the chain fluid of unbonded spheres. This EoS has been applied for H_2-blend mixtures with hydrocarbon [47–49]. The SAFT and similar EoSs are not universal and are mostly restricted to linear alkanes and alkenes. Thus, they may induce undesired numerical pitfalls and often fail to represent the critical zone of pure compounds with reasonable accuracy [50–54]. Therefore, they require fitting using experimental data by regressing the binary interaction parameters (k_{ij}).

The classical EoSs, such as PR and SRK, with or without using k_{ij} coefficients, often fail to accurately predict the phase equilibrium of various gas mixtures with one or more polar components [14]. Therefore, the present work investigates the capability of the latest modification by Schwartzentruber and Renon (1989) using the Redlich–Kwong (1949) EoS (SR-RK) and another type of EoS (PC-SAFT) in predicting the solubility of H_2 in liquid-phase water mixture and water vaporization in gaseous H_2 for a wide range of pressures and temperatures.

Methodology

The workflow approach starts by generating accurate thermodynamic models using a sophisticated regression algorithm with each of the selected EoSs (i.e., SR-RK and PC-SAFT) calibrated against VLE experimental data. Then, a flash liberation simulation was used to calculate the solubility scenarios between H_2O and H_2 using a separator unit in adiabatic conditions. The results were validated against a wide range of conditions found in the collected experimental work. Afterward, the approach was used to assess the influence of potential gas impurity on the solubility calculations over a wide range of temperatures and pressures by introducing CO_2 into the feed gas at different ratios.

The approach used only experimental data with reported uncertainty information. Insufficient data points with high uncertainty were excluded. Moreover, comprehensive objective functions were used to regress the thermodynamic parameters of the models against the experimental data. The parameters with the least root mean square error (RMSE) were used to predict different properties for several isothermal systems. For instance, the error between the experimental mole fraction of component, $y_{i,exp}$ and the calculated mole fraction of component i, $y_{i,cal}$ over the total number of components, n, is given by [55]:

$$RMSE = \sqrt{\sum_{i=1}^{n} \frac{\left(y_{i,exp} - y_{i,cal}\right)^2}{n}}. \tag{1}$$

In this work, Aspen Plus (v. 12.0) [56] was used to validate the models and simulate the solubility behavior of H_2 in water and the water content in the vapor phase of the mixture (i.e., water vaporization). After obtaining the optimized parameters for the EoSs from VLE regression, a flash simulation model was built using Aspen Plus Flowsheet simulation. An adiabatic flash separator at a given temperature and pressure is fed by two streams: H_2 and water. The product streams corresponding to the resulting two phases (vapor and liquid) are measured, as illustrated in Fig. 3.

The statistically most reliable parameter estimates are obtained using the maximum likelihood function (MLF). Assuming that all measurements are independent and that the measurement noise follows a

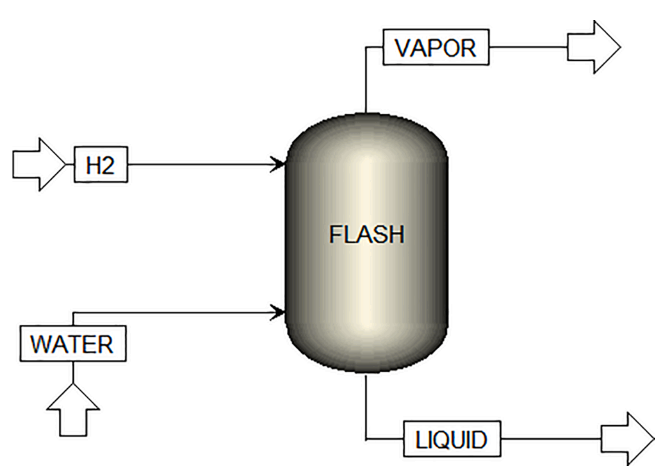

Fig. 3. Flash liberation experiment schematic using Aspen Plus flowsheet simulation (v. 12.0) [56].

Table 1
Alpha functions as a function of reduced temperature ($T_r = T/T_c$) and various parameters (u and w) for the general formalism of the cubic equations of state.

EoS	α(T)	u	w	Ω_a	Ω_b	Reference
Van der Waals	$\alpha(T) = 1$	0	0	0.421875	0.12500	[38]
Redlich–Kwong	$\alpha(T) = 1/\sqrt{T_r}$	1	0	0.427480	0.08664	[39]
Soave Redlich–Kwong	$\alpha(T) = \left[1 + m(\omega)(1-\sqrt{T_r})\right]^2$ $m(\omega) = 0.480 + 1.574\omega - 0.176\omega^2$	1	0	0.427480	0.08664	[30,64,65]
Peng–Robinson	$\alpha(T) = \left[1 + m(\omega)(1-\sqrt{T_r})\right]^2$ $m(\omega) = 0.37464 + 1.54226\omega - 0.26992\omega^2$	2	1	0.457240	0.07780	[29,66]
Boston–Mathias Peng–Robinson*	$\alpha(T) = \begin{cases} \left[1 + m(\omega)\left(1-\sqrt{T_r}\right)\right]^2 & T_r \le 1 \\ e^{[C_d(1-T_r^d)]} & T_r > 1 \end{cases}$ $m(\omega) = 0.37464 + 1.54226\omega - 0.26992\omega^2$ $d = 1 + m/2$ $C_d = \frac{m}{2}$	2	1	0.457240	0.07780	[43,45,62]

* C_d and d are equation parameters.

Gaussian distribution with a zero mean, the MLF can be obtained using a weighted least-squares minimization with weights (w_n) related to the standard deviation (STD) of the measurement. The MLF model incorporates all compositions (liquid-phase mole fraction x and vapor-phase mole fraction y) at a temperature (T) and pressure (P), such that,

$$MLF = \sum_{n=1}^{NG} w_n \sum_{i=1}^{NP} \left[\left(\frac{T_{e,i} - T_{m,i}}{STD_{T,i}}\right)^2 + \left(\frac{P_{e,i} - P_{m,i}}{STD_{P,i}}\right)^2 + \sum_{j=1}^{NC-1} \left(\frac{x_{e,i,j} - x_{m,i,j}}{STD_{y,i,j}}\right)^2 + \sum_{j=1}^{NC-1} \left(\frac{y_{e,i,j} - y_{m,i,j}}{STD_{y,i,j}}\right)^2 \right], \tag{2}$$

where NG is the number of the data group, NP is the number of points in each data group, and NC is the total number of components.

Thermodynamic Modeling Using Equations of State

Cubic Equations of State

The EoSs are semi-empirical correlations that interrelate pressure (P), temperature (T), and volume (V) with the phase composition (x_i) to calculate the thermodynamic behavior of a fluid. In pressure-explicit EoSs, the volume is commonly solved. Then, the rest of the properties are derived [57–59]. A general form of a cubic EoS was suggested by Daridon et al. (1993) [60] based on Schmidt and Wenzel's work (1980) [61], presented as follows:

$$P = \frac{RT}{V_m - b} - \frac{a\alpha(T)}{V_m^2 + ubV_m - wb^2}, \tag{3}$$

where R is the universal gas constant, V_m denotes the molar volume, u and w represent parameters of the generalized EoS, and $\alpha(T)$ is a component function introduced to capture the temperature effect, especially around the critical region. The $\alpha(T)$ function has been extensively assessed by researchers to develop accurate formalisms for different types of fluids with a high consensus level [57,62,63]. The constants a and b are component-dependent, representing the attraction between the molecules and defining the volume of a pure component as a function of the critical temperature (T_c) and critical pressure (P_c), with the following forms:

$$a = \Omega_a \frac{R^2 T_c^2}{P_c}, \tag{4}$$

$$b = \Omega_b \frac{RT_c}{P_c}, \tag{5}$$

where Ω_a and Ω_b represent unitless constants, corresponding to the developed EoS. The forms of the different $\alpha(T)$ functions are summarized in Table 1.

In addition to the above EoSs, the modified SR-RK EoS is also investigated in this work. The main improvement in the SR-RK compared to the classical cubic EoS is achieved by introducing polar parameters in the α function (p_o, p_1, p_2), following the approach by Mathias [45] with the acentric factor (ω) and reduced temperature ($T_r = T/T_c$) (refer to Table 4). The volume translation (c) is used to improve the density predictions. The form proposed by Pilz [57,67] is presented as follows:

$$P = \frac{RT}{V_m + c - b} - \frac{a.\alpha(T)}{(V_m + c)(V_m + c + b)}, \tag{6}$$

$$\alpha(T) = \begin{cases} \left[e^{[C_d(1-T_r^d)]}\right]^2 & T_r > 1 \\ \left[1 + m(\omega)\left(1 - \sqrt{T_r}\right) - p_o(1-T_r)(1 + p_1 T_r + p_2 T_r^2)\right]^2 & T_r \le 1, \end{cases} \tag{7}$$

$$m(\omega) = 0.48508 + 1.55191\omega - 0.15613\omega^2, \tag{8}$$

$$d = 1 + \frac{m}{2} - p_o(1 + p_1 + p_2) \tag{9}$$

$$C_d = 1 - \frac{1}{d}. \tag{10}$$

$$a = \frac{1}{9\left(2^{1/3} - 1\right)} \frac{R^2 T_c^2}{P_c}. \tag{11}$$

$$b = \frac{1}{3}\left(2^{1/3} - 1\right) \frac{RT_c}{P_c} \tag{12}$$

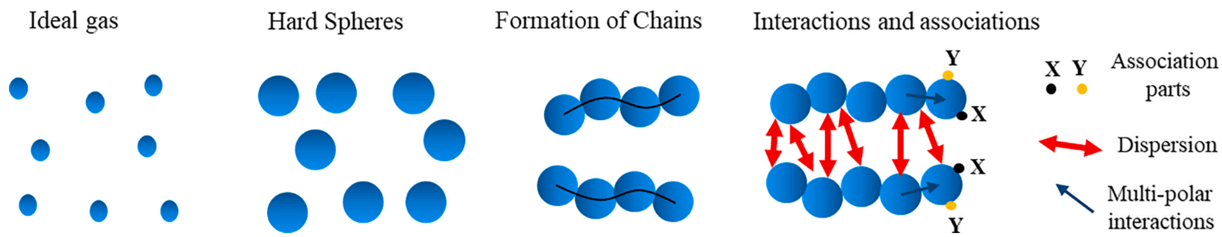

Fig. 4. Molecular model representing the perturbed-chain system in the PC-SAFT, demonstrating different interactions, including dispersion, dipole-dipole, and association.

$$a_{mixture} = \sum_{i=1}^{N} x_i x_j \sqrt{a_i a_j}\left(1 - k_{a,ij} - l_{ij}(x_i - x_j)\right), \tag{13}$$

$$b_{mixture} = \sum_{i=1}^{N}\sum_{j=1}^{N} x_i x_j \frac{b_{i+}b_j}{2}\left(1 - k_{b,ij}\right), \text{ and} \tag{14}$$

$$c_{mixture} = \sum_{i=1}^{N} x_i c_i, \tag{15}$$

The constants a and b, as a function of T_c and P_c, are given by the following:

For mixture calculations, the nonquadratic mixing rule proposed by Schwartzentruber and Renon (1989) [46] is applied with three temperature-dependent binary interaction parameters (k_{aij}, k_{bij}, andl_{ij}), that is,

Where

$$k_{a,ij} = \delta_{a,0} + \delta_{a,1} T + \frac{\delta_{a,2}}{T}, (k_{a,ij} = k_{a,ji}), \tag{16}$$

$$k_{b,ij} = \delta_{b,0} + \delta_{b,1} T + \frac{\delta_{b,2}}{T}, (k_{b,ij} = k_{b,ji}), \tag{17}$$

$$l_{ij} = l_0 + l_1 T + \frac{l_2}{T}, (l_{ij} = -l_{ji}) \tag{18}$$

The binary interaction coefficients, polar parameters, and volume translation ($k_{a,ij}, k_{b,ij}, l_{ij}, p_i$, and$c_i$) are all fine-tuned using experimental data in the reference data section.

PC-SAFT Equation of State

The PC-SAFT is the second type of EoS investigated in this work. The PC-SAFT is based on statistical mechanics similar to any high-order SAFT EoSs [68,69] developed by Gross and Sadowski using the perturbation theory [70,71].

The theoretical bases of SAFT models are based on the first-order perturbation thermodynamic theory of Wertheim [72–74] to develop EoSs, such as those introduced by [75] and [69]. The perturbation-based models are often introduced to represent simplified solutions for a given molecular model. In PC-SAFT, the underlying molecular model is described as a coarse-grained representation of the molecules and their intermolecular interactions, as illustrated in Fig. 4.

The principal idea of using the perturbation solutions is to split the total intermolecular forces into a reference term representing repulsive interactions and a perturbation or correction term that accounts for the attractive forces. The attractive forces are additionally split into various contributors. Theoretically, the first term is known, and the perturbation term is determined as a function of temperature, composition, and pressure or density. Once a perturbation term is selected, the rest of the remaining thermodynamic parameters are estimated using conventional thermodynamic formulations.

The attractive intermolecular forces are further divided into different contributions. The PC-SAFT, similar to many SAFT EoSs, is expressed as an aggregation of the reduced residual Helmholtz free energy (F^{res}) for each contributor term that represents the type of intermolecular force in the system. The residual Helmholtz free energy is the same as the Helmholtz free energy at the same temperature and volume minus the ideal gas Helmholtz free energy. Thus, the molecular interaction forces for a specific number of molecules (N_i) for each individual component, volume (V), and density (ρ) in the PC-SAFT are written as follows:

$$\frac{F^{res}}{N_i k_B T} = \frac{f^{res}}{k_B T} = \frac{f^{hc}}{k_B T} + \frac{f^{hs}}{k_B T} + \frac{f^{disp}}{k_B T} + \frac{f^{assoc}}{k_B T} + \frac{f^{polar}}{k_B T}, \tag{19}$$

where k_B denotes the Boltzmann constant, and the right-hand expression in Eq. (19) represents the hard-chain reference fluid that characterizes the PC-SAFT. The superscripts for the various Helmholtz energy terms denote the contribution from the chain formation (hc), hard-sphere repulsion (hs), and dispersion ($disp$), association ($assoc$), and interpolar ($polar$) interactions, respectively.

In PC-SAFT, three parameters for each pure component are incorporated to account for the nonassociating components: the number of molecular chain segments (M), dispersion energy between segments (ε), and either the diameter of the chain segment (σ) or volume of the chain segment (v^{00}), respectively. For the pure components with association interactions, two more parameters are included: the association volume (κ^{AB}) and association energy between sites, the molecules (ε^{AB}). Following the methodology adopted in this work, the above parameters in PC-SAFT were adjusted to fit the experimental data used for the pure component vapor and liquid saturation pressures.

The PC-SAFT can be extended to mixtures by modifying σ_{mix} and ε_{mix} using mixing rules [69,76] derived from the single-fluid theory by van der Waals, as indicated .below:

$$\sigma_{mix}^3 = \frac{\sum_{i=1}^{n}\sum_{j=1}^{n} x_i M_i x_j M_j \sigma_{ij}^3}{\left(\sum_{i=1}^{n} x_i M_i\right)^2}, \tag{20}$$

$$\varepsilon_{mix}\sigma_{mix}^3 = \frac{\sum_{i=1}^{n}\sum_{j=1}^{n} x_i M_i x_j M_j \varepsilon_{ij}\sigma_{ij}^3}{\left(\sum_{i=1}^{n} x_i M_i\right)^2}. \tag{21}$$

The association parameters, like the dispersion interaction, were calculated using Lorentz–Berthelot combining rules [69,70]. Accordingly, the dispersion cross energy between segments (ε_{ij}) and the diameter of the chain segment (σ_{ij}) are given below:

Table 2
Experimental data for vapor-liquid equilibria (VLE) and solubility for H_2–H_2O mixtures [14].

No.	Reference	Temperature range, K	Pressure range, MPa
1	[77]	273.15–373.15	2.5–101.3
2	[78]	310.93–588.71	0.34–13.79
3	[79]	323.15–423.15	3.18–15.37
4	[80]	366.48–588.7	1.38–11.03
5	[81]	373.15–573.15	2.1–10.0
6	[82]	373.15–498.15	3.1–11.8
7	[83]	310.95–366.45	1.38–13.79
8	[84]	323.15–573.15	5.0–30.0
9	[85]	323.15	10.13–101.33
10	[86]	300–650	0.5–4.5

Table 3
Review of experimental data for vapor-liquid equilibria (VLE) of H_2–CO_2 mixtures.

H_2 mole fraction in liquid phase	T range, K	P range, MPa	References
0.0013-0.4720	219.9–303.1	1.07–96.65	[72,80,90–93,81–85,87–89]

Table 4
Critical properties and acentric factors (ω) for pure components commonly in H_2–blend mixtures [94–98].

Properties	Unit	H_2	H_2O	CO_2	CO
Mw	kg/kmol	2.0159	18.015	44.01	28.01
Tc	K	33.145	647.1	304.13	132.86
Pc	MPa	1.2964	22.064	7.3773	3.494
ρc	kg/m^3	31.262	322.0	467.6	303.91
ω	Unitless	-0.219	0.3443	0.22394	0.0497

Table 5
Adjusted PC-SAFT parameters for components in H_2–H_2O and H_2–CO_2 mixtures.

Component	ε/k(K)	σ(Å)	M
H_2	31.57	3.54	0.68
H_2O	150.17	2.61	2.58
CO_2	86.15	2.84	1.38

$$\varepsilon_{ij} = \left(1 - k_{ij}\right)\sqrt{\varepsilon_i \varepsilon_j}, \tag{22}$$

$$\sigma_{ij} = 0.5\left(\sigma_i + \sigma_j\right). \tag{23}$$

The combining rules incorporate the binary interaction parameter (k_{ij}), allowing a direct comparison with other EoSs used in this work. Additionally, the binary interaction parameter can be used to apply a complex temperature dependence with multiple equation coefficients, such as the one used in this study, using the reduced temperature, as presented below:

$$k_{ij} = a_{ij} + \frac{b_{ij}}{T_r} + c_{ij}\ln T_r + d_{ij}T_r + e_{ij}T_r^2, \tag{24}$$

where a_{ij}, b_{ij}, c_{ij}, d_{ij}, and e_{ij} are equation parameters. The PC-SAFT, similar to the cubic EoSs, requires some optimization of the regression parameters in the binary interaction coefficients, as indicated in Eq. (24).

Reference Data

The thermodynamic properties of H_2–H_2O mixtures have been extensively investigated experimentally since 1927, covering a wide range of temperatures and pressures (up to 573K and 101.33 MPa). Rahbari et al. [14] provided a review of these experimental data (Table 2), which are used to validate H_2–H_2O VLE models in this work.

This work uses the H_2–CO_2–H_2O mixture to demonstrate the influence of impurity with CO_2 on the performance of H_2 solubility in liquid water and water in vapor H_6. The phase equilibrium experimental data for H_2–CO_2 are required to validate thermodynamic models before modeling solubility (see Table 3).

The properties of pure components found in H_2 mixtures concerning the storage process in the investigated EoSs are listed in Table 4. These properties facilitate predicting the thermodynamic behavior of the mixtures using different EoSs. Predictions are calculated by regressing the binary interaction, polar parameters, and volume translation ($k_{a,ij}$, $k_{b,ij}, l_{ij}, p_i$, and c_i) against the experimental data for the considered mixtures.

Table 6
Optimized coefficients of binary interaction parameters in PC-SAFT EoS for H_2–H_2O and H_2–CO_2 mixtures.

H_2 Mixtures	$k_{ij} = a_{ij} + b_{ij}/T_r + c_{ij}\ln T_r + d_{ij}T_r + e_{ij}T_r^2$				
	a_{ij}	b_{ij}	c_{ij}	d_{ij}	e_{ij}
H_2–H_2O	2.262	-2.560	-3.424	0.000	0.000
H_2–CO_2	0.047	-0.017	0.014	0.399	-2.449

Table 7
Optimized coefficients of binary interaction parameters in SR-RK EoS for H_2–H_2O and H_2–CO_2 mixtures.

H_2 Mixtures		H_2–H_2O	H_2–CO_2
$k_{a,ij} = \delta_{a,0} + \delta_{a,1}T + \delta_{a,2}/T$	$\delta_{a,0}$	4.048	1.172
	$\delta_{a,1}$	-0.016	-0.003
	$\delta_{a,2}$	66.576	-69.240
$k_{b,ij} = \delta_{b,0} + \delta_{b,1}T + \delta_{b,2}/T$	$\delta_{b,0}$	17.125	-2.678
	$\delta_{b,1}$	-0.036	0.011
	$\delta_{b,2}$	-1939.77	133.5
$l_{ij} = l_0 + l_1T + l_2/T$	l_0	10.198	-5.891
	l_1	-0.017	0.032
	l_2	-1563.2	252.8

Results and discussion

The calibrated thermodynamic models were first generated using reference data points for the solubility calculations. Predictions were compared to the measurements at high temperatures and pressures to investigate the influence of pressure and temperature on solubility. Then, the influence of H_2 impurity due to CO_2 on solubility at various mixing ratios was assessed.

Regression parameters for H_2–H_2O and H_2–CO_2 mixtures

Regression for key EoS parameters was performed by comparing the calculated VLE envelopes for H_2–H_2O and H_2–CO_2 mixtures with measured reference data points. The selected parameters for the PC-SAFT EoS include ε/k, σ, and M, as listed in Table 5. The final optimized parameters for PC-SAFT (k_{ij}) and SR-RK (k_{aij}, k_{bij}, andl_{ij}) for both mixtures, are presented in Tables 6 and 7, respectively.

The SR-RK and PC-SAFT calculations for VLE diagrams at 367K for H_2–H_2O mixtures are displayed in Fig. 5a and 5b, respectively, where both EoSs obtain a reasonable match with the experimental data. Similarly, for H_2–CO_2 mixtures, the predicted VLE envelopes by the two EoSs agree well with the experimental data, as illustrated in Fig. 6a and 6b.

The RMSE (%) and average absolute deviation (AAD, in %) for the vapor and liquid pressure curves are listed in Table 8 for both mixtures. The results indicate low values for the RMSE (%) and AAD (%), which further support the qualitative matching in Figs. 5 and 6.

The mixing of H_2 and water feeds was simulated using a flash liberation model with a block separator unit under adiabatic conditions. The calculated vapor and liquid streams produced from the separation process were measured following the schematic in Fig. 3. The mixing and separation conditions were selected to mimic the solubility conditions chosen from the experimental reference work in Table 2. The solubility data points are depicted in mole fractions of the liquid H_2 and vapor H_2O measured at various pressures, temperatures, and compositional conditions. The results of the flash calculations at temperatures of 298K, 323K, and 423K are provided in Fig. 7. The figure compares the solubility results calculated using SR-RK and PC-SAFT EoSs against experimental reference data for pressure values of up to 100 MPa. While classical PR and SRK EoSs fail to accurately predict the solubility of H_2

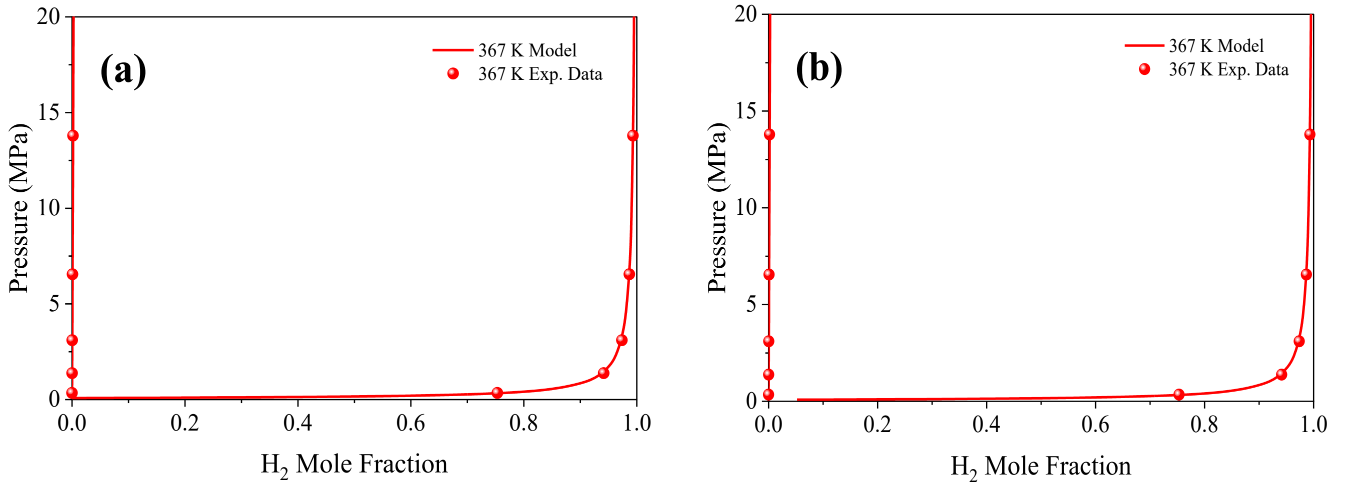

Fig. 5. Experimental data and calculated phase diagrams for H_2–H_2O mixtures at 367K, using thermodynamic models: a) SR-RK and b) PC-SAFT.

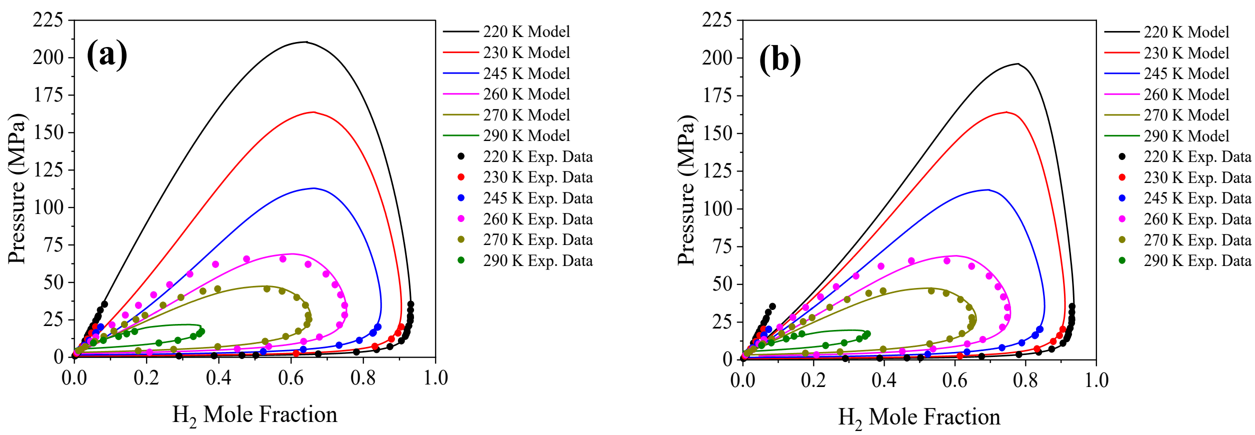

Fig. 6. Predictions of the phase diagrams for H_2–CO_2 mixtures at various temperatures using thermodynamic models: a) SR-RK and b) PC-SAFT.

Table 8
Average absolute deviation (AAD, %) and root mean square error (RMSE, %) of the thermodynamic models using SR-RK and PC-SAFT EoSs for H_2–H_2O and H_2–CO_2 mixtures.

Mixtures	AAD (%) in mixture vapor pressure		AAD% in mixture liquid pressure		RMSE (%)	
	SR-RK	PC-SAFT	SR-RK	PC-SAFT	SR-RK	PC-SAFT
$H_2 - H_2O$	1.84	2.53	0.18	0.24	3.97	4.91
$H_2 - CO_2$	26.8	32.9	1.12	1.04	8.10	8.0

and water vaporization with or without tuning the binary interaction parameters [14], the SR-RK and PC-SAFT EoSs demonstrate their capability to adequately calculate the solubility of H_2 and H_2O at the high temperatures and pressures, as depicted in Fig. 7.

Nevertheless, the accuracy level of the solubility predictions varies with temperature and pressure. At low temperatures, the deviation between the calculated and experimental data for H_2 in H_2O becomes higher as the pressure increases to above 50 MPa. However, the deviation in water vapor at 323K demonstrated a very good match at high pressures, even up to 100 MPa. The predictions follow the trend of the experimental data with acceptable deviation, indicating that both EoSs can be reliable in compositional and engineering simulators. However, careful attention should be exerted while using such models because the validation is only applicable within the considered ranges of pressure, temperature, and compositions in this study.

Effect of temperature and pressure

We studied the influence of temperature and pressure on H_2 solubility and water vaporization. The solubility of gas in water and its relationship to pressure is often expressed by Henry's law, which relates the amount of gas dissolved to the partial pressure of the gas at equilibrium with the liquid [99]. The relationship constant is called Henry's law proportionality constant, symbolized by k_H, and the mathematical formula of Henry's law can be written as follows:

$$P_g = k_H \times c_g, \tag{25}$$

where P_g is the partial pressure of the gas phase, and c_g denotes the volume of dissolved gas in the liquid. The value of k_H depends on the nature of the gas and solvent. The law is only valid for infinite-dilute solutions in equilibrium conditions [100]. The relationship indicates that the solubility of gas increases with increased partial pressure at a constant temperature. However, Henry's law has limitations in modeling solubility under high-pressure conditions or in nonideal fluids [99]. Such nonideal behavior is obtained by the EoSs at high pressure, as observed in Fig. 7a and 7c. An extended version was proposed by [101] for real (nonideal) fluid, formulated to relate the fugacity of the aqueous H_2 ($a_{H_2,aq}$) component to the fugacity of the gaseous H_2 ($a_{H_2,g}$) component at equilibrium, that is,

$$a_{H_2,aq} = K_{@P,T} \times a_{H_2,g}, \tag{26}$$

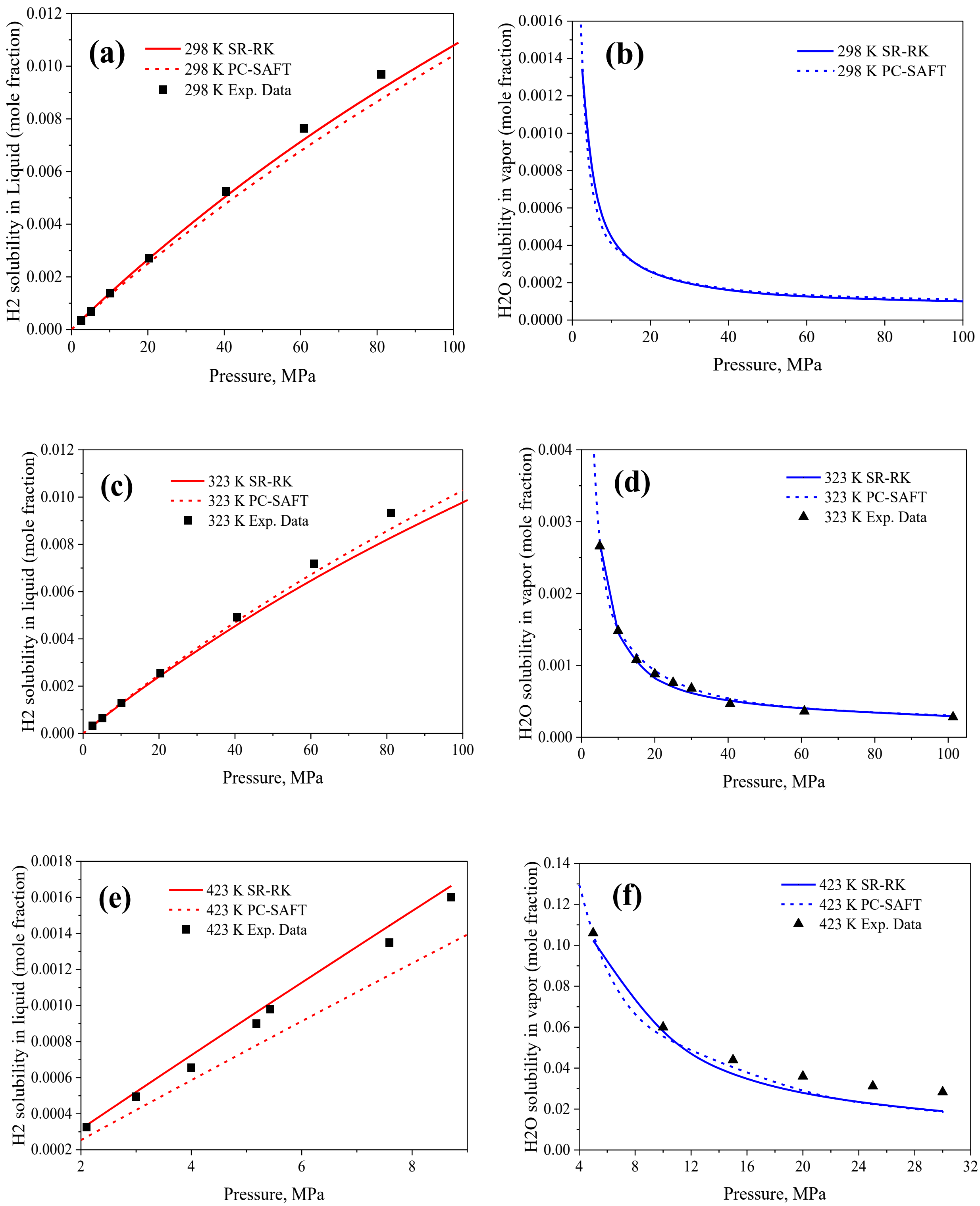

Fig. 7. Solubility of H_2 in liquid water and liquid-water fraction in the produced vapor (i.e., water vaporization) calculated using SR-RK and PC-SAFT, compared to the experimental data at various temperatures: a), c), and e) are H_2 solubility in liquid H_2O at 298K [77], 323K [77], and 423K [79,81], respectively, and b), d), and f) are the H_2O fraction in vapor H_2 at 298K, 323K [84,85], and 423K [84], respectively.

where $K_{@P,T}$ refers to the equilibrium constant of the dissolution of H_2 at specific pressure and temperature values. Pray et al. (1952) experimentally demonstrated the proportional linear relationship between H_2 solubility in pure water and the pressure of various isothermal experimental systems, as predicted by Henry's law (see Fig. 8a). Additionally, solubility was measured at isobaric conditions, capturing some nonlinearity with the temperature at high pressures, as illustrated in Fig. 8b.

In this work, solubility was calculated under the same isothermal conditions using the selected EoSs and was plotted against the experimental data, as displayed in Fig. 9. The models adequately capture the linear trend of the relationship, with better accuracy provided by the SR-

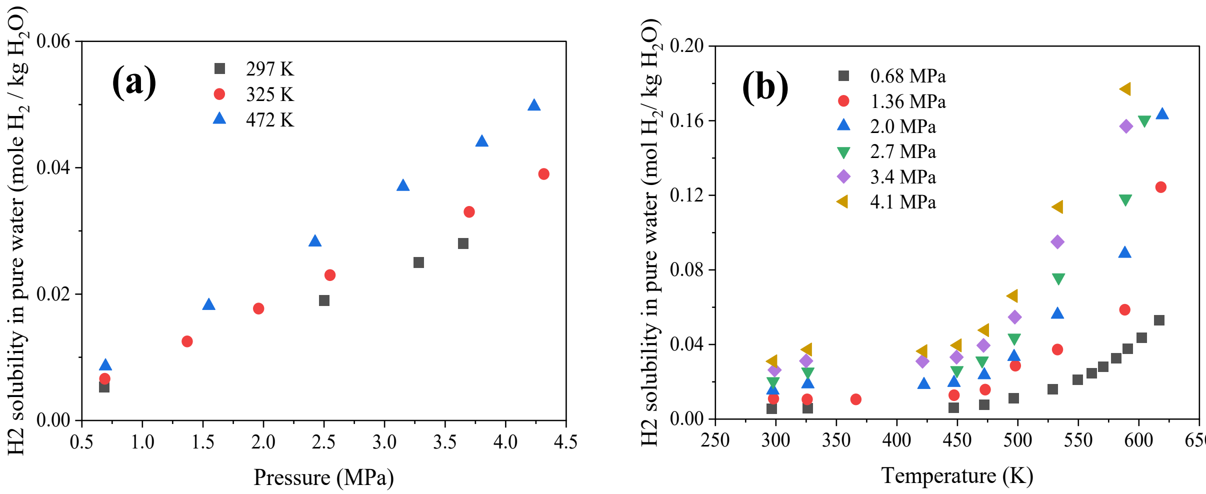

Fig. 8. Experimental solubility measurements of H_2 in pure water by Pray et al. (1952) [86] expressed as a function of a) pressure at isothermal conditions and b) temperature at isobaric conditions.

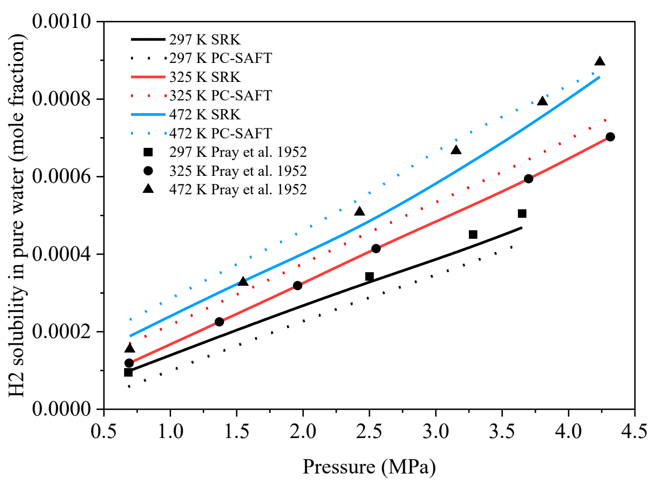

Fig. 9. H_2 solubility in pure water calculated using SR-RK and PC-SAFT, compared to measurements by Pray et al. (1952) in three isothermal conditions (297K, 325K, and 472K). The experimental solubility data were converted from H_2 mole per kilogram of water to the H_2 mole fraction.

RK than the PC-SAFT. Therefore, the SR-RK EoS was selected to study the solubility behavior of H_2 and water content in the vapor phase at high pressures (up to 100 MPa pressure) for three isothermal

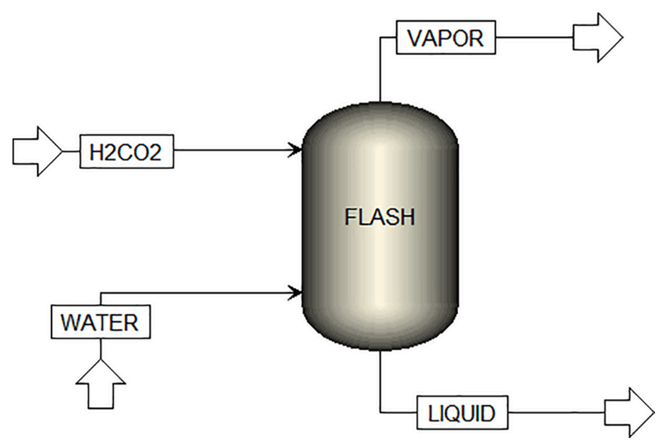

Fig. 11. Flash liberation experiment schematic for the H_2–CO_2 mixture in one feed and the second pure water feed using Aspen Plus flowsheet simulation (v. 12.0) [56].

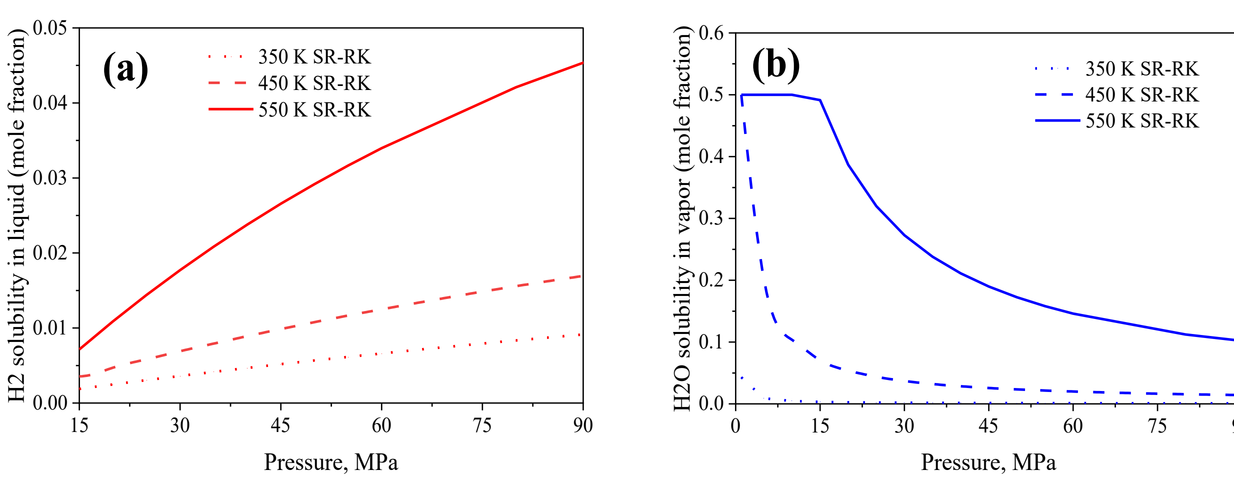

Fig. 10. Solubility calculations from thermodynamic models of H_2 into liquid H_2O and H_2O in vapor H_2 in mole fraction (water vaporization) using SR-RK at 350K, 450K, and 550K extended with pressure: a) solubility of H_2 in liquid H_2O and b) solubility of H_2O liquid in vapor H_2.

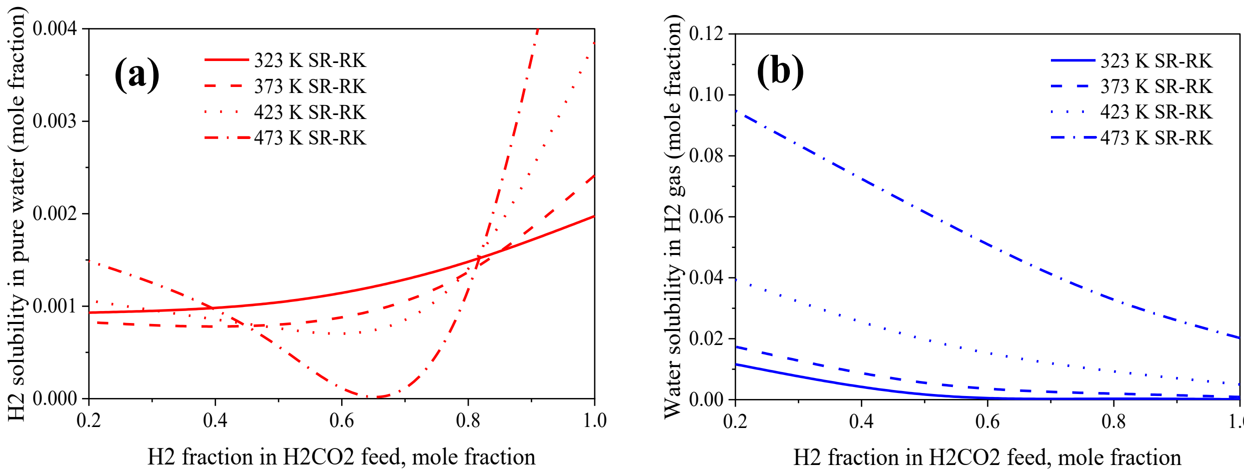

Fig. 12. Plots of the influence of impurity with CO_2 over a wide range of temperatures and at a fixed pressure of 50 MPa on the solubility of a) H_2 in water and b) H_2O vaporization into the gaseous phase.

temperatures (350K, 450K, and 550K), as plotted in Fig. 10.

The plotted solubility in Fig. 10a indicates a proportional relationship with pressure up to approximately 50 MPa, at which the correlation becomes nonlinear, demonstrating the mentioned limitation of Henry's law at higher pressures. The relationship of the water fraction to pressure (Fig. 10b) indicates a sharp decline, with pressure at varying points depending on the temperature condition. Overall, the analysis emphasizes the high sensitivity of the H_2 solubility in pure water and water vaporization at high temperatures and pressures.

Influence of H_2 Impurity

Impurities are commonly found during various H_2 processes, including storage and transportation, such as CH_4, CO_2, N_2, O_2, Ar, and H_2S [15,102]. We investigate the influence of CO_2 (as an example of an impurity) on the solubility of H_2 in liquid H_2O and H_2O content in the vapor phase of the H_2–H_2O mixture.

The solubility calculations were performed using a flash separation model to mix the feed of the H_2–CO_2 mixture in a flash tank under adiabatic conditions with pure water (Fig. 11). The first sensitivity run was performed using SR-RK for a wide range of temperatures from 323K to 473K and at a fixed pressure of 50 MPa.

The results of H_2 solubility in pure water indicate a significant effect of CO_2 on the solubility behavior over a wide range of mixing ratios, as presented in Fig. 12a. In addition, the H_2 solubility profile exhibits strong nonlinearity when the CO_2 concentration in H_2–CO_2 mixture is between 20 % and 60%, particularly at high temperatures, depicting almost opposite behavior for a pure H_2 feed solubility. As illustrated in Fig. 12b, the water vaporization behavior demonstrates a varying decline with temperature. The solubility calculated using SR-RK demonstrates a major influence of impurity by CO_2 and by temperature and pressure on both the H_2 solubility in the liquid phase and the H_2O vaporization behavior.

Conclusion and remarks

The present work proposes a modeling workflow to study the capability of the modified SR-RK cubic EoS and PC-SAFT in predicting the solubility of H_2 in pure liquid H_2O and H_2O vaporization into the gaseous H_2. The results obtained from SR-RK provided very good agreement with the experimental data, a major improvement of the classical cubic EoS. Similarly, PC-SAFT performed very good predictions. The results indicate that both EoSs are reliable to be used for compositional simulators and engineering applications.

Furthermore, the demonstrated regression process provides an approach to better optimize the binary interaction parameters in SR-RK (i.e., k_{aij}, k_{bij}, and l_{ij}) and PC-SAFT (i.e., k_{ij}) for a wide range of pressures (0.34 to 101.23 MPa), temperatures (273.2K to 588.7K), and mole fractions of hydrogen (0.0004 to 0.9670). The flash liberation scenarios were generated using Aspen Plus and evaluated to calculate H_2 solubility and water vaporization of known ratios at adiabatic conditions. The solubility values at different temperature and pressure conditions using SR-RK and PC-SAFT depicted very good predictions of the data trend. The observed deviation from the linear proportionality of the solubility at high pressures (i.e. above 50 MPa) confirms the known limitations of Henry's solubility law at high pressures for nonideal mixtures.

Finally, the influence of CO_2 in the H_2 blend mixture was evaluated to demonstrate the influence of impurity on H_2 solubility in pure water and the water content in the vapor phase at various conditions. The simulated influence of the H_2 solubility profile in water indicates the great influence of impurity due to CO_2 on H_2 solubility and water, particularly at higher temperatures and high mixing ratios.

CRediT authorship contribution statement

Amer Alanazi: Conceptualization, Methodology, Software, Data curation, Writing – original draft. **Saleh Bawazeer:** Visualization, Investigation, Software, Validation. **Muhammad Ali:** Supervision. **Alireza Keshavarz:** Supervision. **Hussein Hoteit:** Supervision, Writing – review & editing.

Declaration of Competing Interest

The authors declare that they have no known competing financial interests or personal relationships that could have appeared to influence the work reported in this paper.

References

[1] Masson-Delmotte V, Zhai P, Pörtner H-O, Roberts D, Skea J, Shukla PR, et al. Summary for policymakers. Global warming of 1.5°C. An IPCC Special Report on the Impacts of Global Warming of 1.5 °C above Pre-industrial Levels. 2018.
[2] Van BJ. The world population explosion: Causes, backgrounds and projections for the future. Facts, Views Vis ObGyn 2013;5:281.
[3] Peterson EWF. The role of population in economic growth. Https://DoiOrg/101177/2158244017736094 2017;7. https://doi.org/10.1177/2158244017736094.
[4] IEA. World energy outlook 2018: Highlights. Int Energy Agency 2018;1.
[5] Moustakas K, Loizidou M, Rehan M, Nizami AS. A review of recent developments in renewable and sustainable energy systems: Key challenges and future perspective. Renew Sustain Energy Rev 2020;119. https://doi.org/10.1016/j.rser.2019.109418.

[6] Cuce E, Harjunowibowo D, Cuce PM. Renewable and sustainable energy saving strategies for greenhouse systems: a comprehensive review. Renew Sustain Energy Rev 2016;64. https://doi.org/10.1016/j.rser.2016.05.077.

[7] Edelenbosch OY, McCollum DL, van Vuuren DP, Bertram C, Carrara S, Daly H, et al. Decomposing passenger transport futures: Comparing results of global integrated assessment models. Transp Res Part D Transp Environ 2017;55. https://doi.org/10.1016/j.trd.2016.07.003.

[8] Lazarou S, Vita V, Diamantaki M, Karanikolou-Karra D, Fragoyiannis G, Makridis S, et al. A simulated roadmap of hydrogen technology contribution to climate change mitigation based on representative concentration pathways considerations. Energy Sci Eng 2018;6. https://doi.org/10.1002/ese3.194.

[9] Hanley ES, Deane JP, Gallachóir BPÓ. The role of hydrogen in low carbon energy futures–A review of existing perspectives. Renew Sustain Energy Rev 2018;82. https://doi.org/10.1016/j.rser.2017.10.034.

[10] McPherson M, Johnson N, Strubegger M. The role of electricity storage and hydrogen technologies in enabling global low-carbon energy transitions. Appl Energy 2018;216. https://doi.org/10.1016/j.apenergy.2018.02.110.

[11] Mahlia TMI, Saktisahdan TJ, Jannifar A, Hasan MH, Matseelar HSC. A review of available methods and development on energy storage. Technology Update. vol. 33. Elsevier Ltd; 2014.

[12] Gallo AB, Simões-Moreira JR, Costa HKM, Santos MM, Moutinho dos Santos E. Energy storage in the energy transition context: A technology review. vol. 65. Elsevier Ltd; 2016.

[13] Chen H, Song J, Zhao J. Synergies between power and hydrogen carriers using fuel-cell hybrid electrical vehicle and power-to-gas storage as new coupling points. Energy Convers Manag 2021;246. https://doi.org/10.1016/j.enconman.2021.114670.

[14] Rahbari A, Brenkman J, Hens R, Ramdin M, van den Broeke LJP, Schoon R, et al. Solubility of water in hydrogen at high pressures: a molecular simulation study. J Chem Eng Data 2019;64:4103–15. https://doi.org/10.1021/ACS.JCED.9B00513.

[15] Heinemann N, Alcalde J, Miocic JM, Hangx SJT, Kallmeyer J, Ostertag-Henning C, et al. Enabling large-scale hydrogen storage in porous media – the scientific challenges. Energy Environ Sci 2021;14:853–64. https://doi.org/10.1039/D0EE03536J.

[16] Møller KT, Jensen TR, Akiba E, Li H wen. Hydrogen – A sustainable energy carrier. Prog Nat Sci Mater Int 2017;27:34–40. https://doi.org/10.1016/J.PNSC.2016.12.014.

[17] Felderhoff M, Weidenthaler C, Von Helmolt R, Eberle U. Hydrogen storage: the remaining scientific and technological challenges. Phys Chem Chem Phys 2007;9:2643–53. https://doi.org/10.1039/B701563C.

[18] Kirtay E. Recent advances in production of hydrogen from biomass. Energy Convers Manag 2011;52:1778–89. https://doi.org/10.1016/j.enconman.2010.11.010.

[19] Bouwman P. Electrochemical Hydrogen Compression (EHC) solutions for hydrogen infrastructure. Fuel Cells Bull 2014;2014:12–6. https://doi.org/10.1016/S1464-2859(14)70149-X.

[20] Hogerwaard J, Dincer I, Naterer GF. Experimental investigation and optimization of integrated photovoltaic and photoelectrochemical hydrogen generation. Energy Convers Manag 2020;207. https://doi.org/10.1016/j.enconman.2020.112541.

[21] Bhattacharyya R, Misra A, Sandeep KC. Photovoltaic solar energy conversion for hydrogen production by alkaline water electrolysis: Conceptual design and analysis. Energy Convers Manag 2017;133:1–13. https://doi.org/10.1016/j.enconman.2016.11.057.

[22] Taylor JB, Alderson JEA, Kalyanam KM, Lyle AB, Phillips LA. Technical and economic assessment of methods for the storage of large quantities of hydrogen. Int J Hydrogen Energy 1986;11. https://doi.org/10.1016/0360-3199(86)90104-7.

[23] Crotogino F, Donadei S, Bünger U, Landinger H. Large-scale hydrogen underground storage for securing future energy supplies. 18th World Hydrog Energy Conf 2010 – WHEC 2010 Parallel Sess B 4 Storage Syst/Policy Perspect Initiat Co-Operations 2010;78.

[24] Panfilov M. Underground storage of hydrogen: In situ self-organisation and methane generation. Transp Porous Media 2010;85. https://doi.org/10.1007/s11242-010-9595-7.

[25] Flanigan O. Underground gas storage facilities: Design and implementation. Elsevier; 1995.

[26] Shao H, Kukkadapu RK, Krogstad EJ, Newburn MK, Cantrell KJ. Mobilization of metals from Eau Claire siltstone and the impact of oxygen under geological carbon dioxide sequestration conditions. Geochim Cosmochim Acta 2014;141. https://doi.org/10.1016/j.gca.2014.06.011.

[27] Seward TM, Franck EU. System hydrogen-water up to 440°C and 2500 bar pressure. Berichte Der Bunsengesellschaft/Physical Chem Chem Phys 1981;85. https://doi.org/10.1002/bbpc.19810850103.

[28] Michels A, Goudeket M. Equ of hydrogen between 0°C and 150°C up to 3000 atmospheres. Physica 1941;8. https://doi.org/10.1016/S0031-8914(41)90076-9.

[29] Peng DY, Robinson DB. A new two-constant equation of state. Ind Eng Chem Fundam 1976;15:59–64. https://doi.org/10.1021/i160057a011.

[30] Soave G. Equilibrium constants from a modified Redlich-Kwong equation of state. Chem Eng Sci 1972;27:1197–203. https://doi.org/10.1016/0009-2509(72)80096-4.

[31] Firoozabadi A. Thermodynamics of hydrocarbon reservoirs. McGraw-Hill 1999. https://doi.org/10.1016/j.ecolind.2015.10.046.

[32] Li H. Thermodynamic properties of CO_2 mixtures and their applications in advanced power cycles with CO_2 capture processes. PhD Thesis R Institute Technology 2008:1–63.

[33] Carroll JJ. Acid gas injection and carbon dioxide sequestration. 2010. doi: 10.1002/9780470893210.

[34] Wei Y, Chen Z, Satyro M, Dong C, Deng H. Compositional simulation using the advanced Peng-Robinson equation of state. Soc. Pet. Eng. - SPE Reserv Simul Symp 2011;2:2011. https://doi.org/10.2118/141898-ms.

[35] Hoteit H, Firoozabadi A. Compositional modeling of discrete-fractured media without transfer functions by the discontinuous Galerkin and mixed methods. SPE J 2006;11:341–52. https://doi.org/10.2118/90277-PA.

[36] Hoteit H, Firoozabadi A. Modeling of multicomponent diffusions and natural convection in unfractured and fractured media by discontinuous Galerkin and mixed methods. Int J Numer Methods Eng 2018;114:535–56. https://doi.org/10.1002/nme.5753.

[37] Sadus RJ. Influence of quantum effects on the high-pressure phase behavior of binary mixtures containing hydrogen. J Phys Chem 1992;96. https://doi.org/10.1021/j100188a052.

[38] van der Waals JD. Over de continuiteit van den gas- en vloeistoftoest. 1873.

[39] Redlich O, Kwong JNS. On the thermodynamics of solutions. V. An equation of state. Fugacities of gaseous solutions. Chem Rev 1949;44. https://doi.org/10.1021/cr60137a013.

[40] Wilson GM. Vapor-liquid equilibria, correlation by means of a modified Redlich-Kwong equation of state. Adv Cryog Eng 1964:168–76. https://doi.org/10.1007/978-1-4757-0525-6_21.

[41] Joffe J. Vapor-liquid equilibria and densities with the Martin equation of state. Ind Eng Chem Process Des Dev 1981;20. https://doi.org/10.1021/i200012a027.

[42] Martin JJ. Cubic equations of state–Which? Ind Eng Chem Fundam 1979;18:81.

[43] Boston JF, Mathias PM. Phase equilibria in a third-generation process simulator. EFCE Publ Ser European Fed Chem Eng 1980.

[44] Mathias PM, Klotz HC, Prausnitz JM. Equation-of-State mixing rules for multicomponent mixtures: the problem of invariance. Fluid Phase Equilib 1991;67. https://doi.org/10.1016/0378-3812(91)90045-9.

[45] Mathias PM. A versatile phase equilibrium equation of state. Ind Eng Chem Process Des Dev 1983;22. https://doi.org/10.1021/i200022a008.

[46] Schwartzentruber J, Renon H. Extension of UNIFAC to high pressures and temperatures by the use of a cubic equation of state. Ind Eng Chem Res 1989;28. https://doi.org/10.1021/ie00091a026.

[47] Ghosh A, Chapman WG, French RN. Gas solubility in hydrocarbons – a SAFT-based approach. Fluid Phase Equilib 2003;209:229–43. https://doi.org/10.1016/S0378-3812(03)00147-X.

[48] Florusse LJ, Peters CJ, Pàmies JC, Vega LF, Meijer H. Solubility of hydrogen in heavy n-alkanes: experiments and SAFT modeling. AIChE J 2003;49. https://doi.org/10.1002/aic.690491225.

[49] Tran TKS, NguyenHuynh D, Ferrando N, Passarello JP, De Hemptinne JC, Tobaly P. Modeling VLE of H 2 + hydrocarbon mixtures using a group contribution saft with a *kij* correlation method based on London's theory. Energy and Fuels 2009;23:2658–65. https://doi.org/10.1021/EF801101Z/SUPPL_FILE/EF801101Z_SI_001.PDF.

[50] Kalikhman V, Kost D, Polishuk I. About the physical validity of attaching the repulsive terms of analytical EOS models by temperature dependencies. Fluid Phase Equilib 2010;293. https://doi.org/10.1016/j.fluid.2010.03.003.

[51] Polishuk I. Addressing the issue of numerical pitfalls characteristic for SAFT EOS models. Fluid Phase Equilib 2011;301:123–9. https://doi.org/10.1016/j.fluid.2010.11.021.

[52] Polishuk I. About the numerical pitfalls characteristic for SAFT EOS models. Fluid Phase Equilib 2010;298:67–74. https://doi.org/10.1016/j.fluid.2010.07.003.

[53] Privat R, Conte E, Jaubert JN, Gani R. Are safe results obtained when SAFT equations are applied to ordinary chemicals? Part 2: Study of solid-liquid equilibria in binary systems. Fluid Phase Equilib 2012;318. https://doi.org/10.1016/j.fluid.2012.01.013.

[54] Privat R, Gani R, Jaubert JN. Are safe results obtained when the PC-SAFT equation of state is applied to ordinary pure chemicals? Fluid Phase Equilib 2010;295. doi: 10.1016/j.fluid.2010.03.041.

[55] Barker JA. Determination of activity coefficients from total pressure measurements. Aust J Chem 1953;6. https://doi.org/10.1071/CH9530207.

[56] Aspen Technology Inc. Aspen Plus ® User Guide. 2015.

[57] Mangold F, Pilz S, Bjelić S, Vogel F. Equation of state and thermodynamic properties for mixtures of H_2O, O_2, N_2, and CO_2 from ambient up to 1000K and 280 MPa. J Supercrit Fluids 2019;153. https://doi.org/10.1016/j.supflu.2019.02.016.

[58] Reid RC, Prausnitz JM, Poling BE. The properties of gases and liquids 1987.

[59] Balaji B, Vasudevan R, Ramamurthi K. A Parametric study of the choice of binary interaction parameter and equation of state for high pressure vapor-liquid equilibrium of nitrogen - N-dodecane binary system. Int J Thermodyn 2011;14. https://doi.org/10.5541/ijot.277.

[60] Daridon JL, Saint-Guirons H, Lagourette B, Xans P, Leibovici C. A generalized process for phase equilibrium calculation with cubic equations of state. Int J Thermophys 1993;14.

[61] Schmidt G, Wenzel H. A modified van der Waals type equation of state. Chem Eng Sci 1980;35:1503–12. https://doi.org/10.1016/0009-2509(80)80044-3.

[62] Mathias PM, Copeman TW. Extension of the Peng-Robinson equation of state to complex mixtures: Evaluation of the various forms of the local composition concept. Fluid Phase Equilib 1983;13. https://doi.org/10.1016/0378-3812(83)80084-3.

[63] Twu CH, Bluck D, Cunningham JR, Coon JE. A cubic equation of state with a new alpha function and a new mixing rule. Fluid Phase Equilib 1991;69. https://doi.org/10.1016/0378-3812(91)90024-2.
[64] Graboskl MS, Daubert TE. A modified soave equation of state for phase equilibrium calculations. 2. Systems containing CO_2, H_2S, N_2, and CO. Ind Eng Chem Process Des Dev 1978;17:448–54. https://doi.org/10.1021/I260068A010.
[65] Kabadi VN, Danner RP. A modified Soave–Redlich–Kwong equation of state for water-hydrocarbon phase equilibria. Ind Eng Chem Process Des Dev 1985;24. https://doi.org/10.1021/i200030a004.
[66] Abbott MM. Cubic equations of state: An interpretive review. In Equations of state in engineering reseach. KC Chao, RL Robinson (eds.), Washington, DC, USA, Am Chem Soc, 1979;182:47–70. doi: 10.1021/BA-1979-0182.CH003.
[67] Pilz S. Investigations by computation and experiments on a supercritical water oxidation application treating solid residues of electronic scrap. 2006.
[68] Huang SH, Radosz M. Equation of state for small, large, polydisperse, and associating molecules: extension to fluid mixtures. Ind Eng Chem Res 1991;30. https://doi.org/10.1021/ie00056a050.
[69] Chapman WG, Gubbins KE, Jackson G, Radosz MSAFT. Equation-of-state solution model for associating fluids. Fluid Phase Equilib 1989;52. https://doi.org/10.1016/0378-3812(89)80308-5.
[70] Gross J, Sadowski G. Perturbed-chain SAFT: An equation of state based on a perturbation theory for chain molecules. Ind Eng Chem Res 2001;40:1244–60. https://doi.org/10.1021/IE0003887.
[71] Tumakaka F, Gross J, Sadowski G. Thermodynamic modeling of complex systems using PC-SAFT. Fluid Phase Equilib 2005;228–229:89–98. https://doi.org/10.1016/J.FLUID.2004.09.037.
[72] Wertheim MS. Fluids with highly directional attractive forces. IV. Equilibrium polymerization. J Stat Phys 1986;42:477–92. https://doi.org/10.1007/BF01127722.
[73] Wertheim MS. Fluids with highly directional attractive forces. II. Thermodynamic perturbation theory and integral equations. J Stat Phys 1984;35:35–47. https://doi.org/10.1007/BF01017363.
[74] Wertheim MS. Fluids with highly directional attractive forces. I. Statistical thermodynamics. J Stat Phys 1984;35:19–34. https://doi.org/10.1007/BF01017362.
[75] Jackson G, Chapman WG, Gubbins KE. Phase equilibria of associating fluids spherical molecules with multiple bonding sites. Mol Phys 1988;65:1–31. https://doi.org/10.1080/00268978800100821.
[76] Chapman WG, Jackson G, Gubbins KE. Phase equilibria of associating fluids. Http://DxDoiOrg/101080/00268978800101601 2006;65:1057–79. https://doi.org/10.1080/00268978800101601.
[77] Wiebe R, Gaddy VL. The solubility of hydrogen in water at 0, 50, 75 and 100° from 25 to 1000 atmospheres. J Am Chem Soc 1934;56:76–9. https://doi.org/10.1021/JA01316A022.
[78] Gillespie P, Wilson G. Vapor-liquid equilibrium data on water-substitute gas components: N/sub 2/-H/sub 2/O, H/sub 2/-H/sub 2/O, CO-H/sub 2/O, H/sub 2/-CO-H/sub 2/O, and H/sub 2/S-H/sub 2/O (Technical Report) | OSTI.GOV. 1980.
[79] Kling G, Maurer G. The solubility of hydrogen in water and in 2-aminoethanol at temperatures between 323K and 423K and pressures up to 16 MPa. J Chem Thermodyn 1991;23:531–41. https://doi.org/10.1016/S0021-9614(05)80095-3.
[80] Devaney WE, Pen-Li-Kao BJM. High-temperature V-L-E measurements for substitute gas components. Proceedings Annu Conv – Gas Process Assoc 1977.
[81] Jung J, Knacke O, Neuschütz D. Löslichkeit von Kohlenmonoxid und Wasserstoff in Wasser bis 300°C. Chemie Ing Tech 1971;43:112–6. https://doi.org/10.1002/CITE.330430304.
[82] Ipatev V, Teodorovich V. Equilibrium compositions of vapor-gas mixtures over solutions. 1934.
[83] Ugrozov VV. Equilibrium compositions of vapor-gas mixtures over solutions. Russ. J Phys Chem A 1996;70.
[84] Maslennikova VY, Goryunova NP, Subbotina LA, Tsiklis DS. Solubility of water in compressed hydrogen. Zh Fiz Khim 1976;50.
[85] Bartlett EP. The concentration of water vapor in compressed hydrogen, nitrogen and a mixture of these gases in the presence of condensed water. J Am Chem Soc 1927;49:58–65. https://doi.org/10.1021/JA01400A010.
[86] Pray HA, Schweickert CE, Minnich BH. Solubility of hydrogen, oxygen, nitrogen, and helium in water at elevated temperatures. Ind Eng Chem 1952;44. https://doi.org/10.1021/ie50509a058.
[87] Nelson EE, Bonnell WS. Solubility of hydrogen in n-butane. Ind Eng Chem 1943;35. https://doi.org/10.1021/ie50398a016.
[88] Bartlett EP. The compressibility isotherms of hydrogen, nitrogen and mixtures of these gases at 0° and pressures to 1000 atmospheres. A correction. This J 1927;49.
[89] Tsang CY, Streett WB. Phase equilibria in the H_2□CO system at temperatures from 70 to 125K and pressures to 53 MPa. Fluid Phase Equilib 1981;6:261–73. https://doi.org/10.1016/0378-3812(81)85008-X.
[90] Omar MH, Dokoupil Z. Some supplementary measurements on the vapour-liquid equilibrium of the system hydrogen-nitrogen at temperatures higher than the triple point of nitrogen. Physica 1962;28. https://doi.org/10.1016/0031-8914(62)90089-7.
[91] Cipollina A, Anselmo R, Scialdone O, Filardo G, Galia A. Experimental P-T-ρ measurements of supercritical mixtures of carbon dioxide, carbon monoxide, and hydrogen and semiquantitative estimation of their solvent power using the solubility parameter concept. J Chem Eng Data 2007;52:2291–7. https://doi.org/10.1021/JE700307R/SUPPL_FILE/JE700307R2.PDF.
[92] Townend DTA, Bhatt LA. Isotherms of hydrogen, carbon monoxide and their mixtures. Proc R Soc London Ser A, Contain Pap a Math Phys Character 1931;134:502–12. https://doi.org/10.1098/RSPA.1931.0210.
[93] van Itterbeek A, van Paemel O, van Lierde J. Measurements on the thermal diffusion in gas mixtures at low temperatures. Physica 1947;13. https://doi.org/10.1016/0031-8914(47)90081-5.
[94] Kunz O, Wagner W. The GERG-2008 wide-range equation of state for natural gases and other mixtures: an expansion of GERG-2004. J Chem Eng Data 2012;57. https://doi.org/10.1021/je300655b.
[95] Leachman JW, Jacobsen RT, Penoncello SG, Lemmon EW. Fundamental equations of state for parahydrogen, normal hydrogen, and orthohydrogen. J Phys Chem Ref Data 2009;38. https://doi.org/10.1063/1.3160306.
[96] Lemmon EW, Span R. Short fundamental equations of state for 20 industrial fluids. J Chem Eng Data 2006;51:785–850.
[97] Lemmon EW, Bell IH, Huber ML, McLinden MO. NIST reference fluid thermodynamic and transport properties database (REFPROP), Version 10.0; Standard reference data; National Institute of Standards and Technology: Gaithersburg, MD. NIST Stand Ref Databasev23 2018.
[98] Lemmon EW, McLinden MO, Friend D. Thermophysical properties of fluid systems. NIST Chem WebBook. NIST Stand Ref Database Number 2017;69.
[99] Morris DR, Yang L, Giraudeau F, Sun X, Steward FR. Henry's law constant for hydrogen in natural water and deuterium in heavy water. Phys Chem Chem Phys 2001;3:1043–6. https://doi.org/10.1039/B007732L.
[100] Sander R. Compilation of Henry's law constants (version 4.0) for water as solvent. Atmos Chem Phys 2015;15:4399–981. https://doi.org/10.5194/ACP-15-4399-2015.
[101] Lassin A, Dymitrowska M, Azaroual M. Hydrogen solubility in pore water of partially saturated argillites: application to Callovo-Oxfordian clayrock in the context of a nuclear waste geological disposal. Phys Chem Earth 2011;36. https://doi.org/10.1016/j.pce.2011.07.092.
[102] Li H, Yan J. Evaluating cubic equations of state for calculation of vapor-liquid equilibrium of CO_2 and CO_2-mixtures for CO_2 capture and storage processes. Appl Energy 2009;86:826–36. https://doi.org/10.1016/J.APENERGY.2008.05.018.